

## Activated vibrational modes and Fermi resonance in tip-enhanced Raman spectroscopy

Mengtao Sun,<sup>1</sup> Yurui Fang,<sup>1</sup> Zhenyu Zhang,<sup>2,3</sup> and Hongxing Xu<sup>1,4,5,\*</sup>

<sup>1</sup>Beijing National Laboratory for Condensed Matter Physics, Institute of Physics, Chinese Academy of Sciences, P.O. Box 603-146, Beijing 100190, People's Republic of China

<sup>2</sup>ICQD, Hefei National Laboratory at the Microscale, University of Science and Technology of China, Hefei, People's Republic of China

<sup>3</sup>Department of Physics and Astronomy, University of Tennessee, Knoxville, Tennessee 37996-1200, USA

<sup>4</sup>Division of Solid State Physics, Lund University, Lund 22100, Sweden

<sup>5</sup>The Center of Nanoscience and Technology and School of Physics and Technology, Wuhan University, Wuhan 430072, People's Republic of China

(Received 23 August 2011; revised manuscript received 23 January 2013; published 13 February 2013)

Using *p*-aminothiophenol (PATP) molecules on a gold substrate and high-vacuum tip-enhanced Raman spectroscopy (HV-TERS), we show that the vibrational spectra of these molecules are distinctly different from those in typical surface-enhanced Raman spectroscopy. Detailed first-principles calculations help to assign the Raman peaks in the TERS measurements as Raman-active and IR-active vibrational modes of dimercaptoazobenzene (DMAB), providing strong spectroscopic evidence for the dimerization of PATP molecules to DMAB under the TERS setup. The activation of the IR-active modes is due to enhanced electromagnetic field gradient effects within the gap region of the highly asymmetric tip-surface geometry. Fermi resonances are also observed in HV-TERS. These findings help to broaden the versatility of TERS as a promising technique for ultrasensitive molecular spectroscopy.

DOI: [10.1103/PhysRevE.87.020401](https://doi.org/10.1103/PhysRevE.87.020401)

PACS number(s): 33.20.Fb, 68.37.Uv, 68.43.Pq, 73.20.Mf

First demonstrated by Stöckle *et al.*, Hayazawa *et al.*, and Anderson in 2000 [1–3], tip-enhanced Raman spectroscopy (TERS) is a high-sensitivity optical analytical technique, with high spatial resolution beyond the diffraction limit of light. In TERS, a sharp metal tip is used to create a “hot site” to excite localized surface plasmons and, consequently, enhance the electromagnetic field and Raman signals in the vicinity of the tip apex [1–9]. The tip can be moved in three dimensions to control the position of the hot site and the corresponding enhancement factor by changing the distance of the gap between the tip and the substrate. Therefore, TERS has the inherent advantage of overcoming one of the most severe restrictions in the application of surface-enhanced Raman scattering (SERS), which usually requires roughness of metal surfaces or aggregations of metal nanoparticles to create hot sites that are difficult to control. TERS may solve a wide variety of problems in high-vacuum (HV) single-crystal surface science, electrochemistry, heterogeneous catalysis, microelectronics, and tribology, offering new opportunities for gaining insights into the physics and chemistry of these diverse systems.

As a compelling and challenging example, the appearance of normally unseen Raman modes in the spectrum of *p*-aminothiophenol (PATP) adsorbed on metal surfaces has been a long-standing issue in SERS. Earlier explanations often attribute this phenomenon to selective enhancement of some  $b_2$  modes of PATP due to charge transfer between the molecules and the metal substrates [10–13]. Recently, dimerization of PATP to dimercaptoazobenzene (DMAB) has been suggested to explain these unseen Raman modes [14–18]. Both theoretical simulations [14,15] and experimental observations [15,16] offer credible support to the explanation based on the

dimerization mechanism; nevertheless, controversies remain regarding the dimerization explanation due to the broadening and relatively few Raman modes in the SERS spectra [19–21]. It has been suggested that the gradient effect associated with the strongly enhanced electric field at a rough metal surface [22–24] could activate IR-active modes, which are usually Raman inactive. If the IR-active modes of DMAB are observed together with the Raman-active modes in SERS studies, it is expected that the dimerization picture will show more convincing spectroscopic evidence.

In this Rapid Communication, we exploit the advantage of TERS to investigate the long-standing issue of the appearance of new Raman modes of adsorbed PATP molecules, which are typically unseen in normal Raman spectroscopy. We observe many more and narrower Raman peaks in our high-vacuum TERS (HV-TERS) system than in previous SERS studies. By comparing these experimental observations with our theoretical simulations within density functional theory, we can assign almost all the Raman peaks as Raman-active symmetric modes and IR-active asymmetric modes of the DMAB molecule. The fully activated and strongly enhanced IR-active modes as observed in our HV-TERS data give more convincing spectroscopic evidence to support the conversion of PATP via dimerization into the putative product DMAB. The gradient effect associated with the greatly enhanced electric field within the nanogap region between the sharp gold tip and gold film can activate the IR-active modes of the DMAB molecule to be Raman active. The huge electromagnetic enhancement in the nanogap region further results in distinct Fermi resonances, the strong coupling of a fundamental mode and an overtone of a different mode or a combinational mode, to split the corresponding fundamental Raman modes.

The schematic diagram of the HV-TERS system is shown in Fig. 1. It consists of a homemade scanning tunneling microscope (STM) in a high-vacuum chamber, a Raman

\*Corresponding author: [hxxu@iphy.ac.cn](mailto:hxxu@iphy.ac.cn)

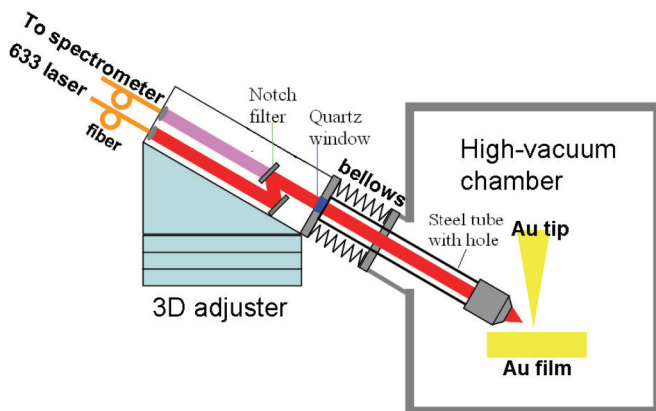


FIG. 1. (Color online) Schematic diagram of the home-built HV-TERS setup.

spectrometer combined with side illumination of 632.8 nm He-Ne laser light with an angle of  $60^\circ$  for Raman measurements, and three-dimensional piezo stages for the tip and sample manipulations. The pressure in the chamber is  $\sim 10^{-7}$  Pa. A gold tip with a  $\sim 50$  nm radius was fabricated by electrochemical etching of a 0.25 mm diameter gold wire [25]. The substrate was prepared by evaporating a 100 nm gold film to a newly cleared mica film under high vacuum. The film was immersed in a  $1 \times 10^{-5}$  M PATP ethanol solution for 24 h, then washed with ethanol for 10 min to guarantee that there was only one monolayer of PATP molecules adsorbed on the gold film. Then, immediately, the sample was put into the high-vacuum chamber. To get a good signal-to-noise ratio, the TERS signals were collected with an acquisition time of 60 s and accumulated 20 times for each spectrum.

We measured TERS of PATP adsorbed on the Au film at different bias voltages and currents and found the optimal conditions to be  $\pm 1$  V (bias voltage on the sample) and 1 nA (current) in our HV-TERS system. Two series of typical measured spectra using the experimental conditions described above for different biases are shown in Figs. 2(a) and 2(b). The fluctuations of these spectra are small, and the spectra are stable and can be readily repeated experimentally under these conditions. The profiles of the spectra obtained at +1 V and -1 V are quite similar, indicating that there is not much influence from the polarity of the bias voltage on the TERS measurement here. For comparison, the typical SERS spectrum of PATP in Au sol and the normal Raman scattering (NRS) spectrum of PATP powder [Fig. 2(c)] were also measured with a Renishaw inVia Raman system and excited with light at 632.8 nm. The molecular structures of DMAB and PATP are also shown in the insets of Fig. 2(c).

Comparing Figs. 2(a) and 2(b) with Fig. 2(c), it is found that the TERS peaks of PATP adsorbed on the Au film are significantly different from the SERS and NRS peaks of PATP. Many more and narrower Raman peaks are observed in Figs. 2(a) and 2(b) for the HV-TERS study than in Fig. 2(c) for the SERS and NRS studies. It is worthwhile to note that our previous report showed that the SERS peaks of PATP adsorbed on a bare Au film are very similar to the NRS of PATP [18], whereas the SERS peaks of PATP on Au colloidal nanoparticles are different from the corresponding

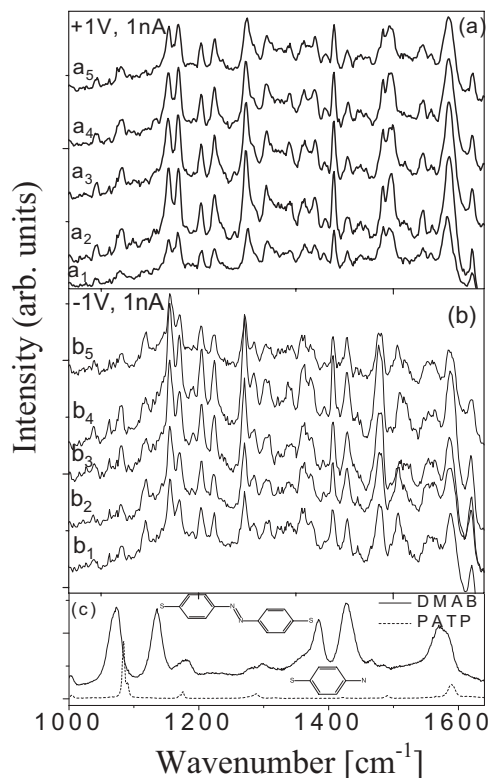


FIG. 2. Spectra of DMAB under experimental conditions of 1 nA current and (a) +1 V, and (b) -1 V bias voltage, measured at different positions with the HV-TERS system. (c) SERS peaks of DMAB in Au sol and the normal Raman scattering spectrum of PATP.

NRS measurements. The latter case has been attributed to plasmon-assisted chemical reaction of PATP dimerization into DMAB, but that is not the case for the bare Au film where the plasmon enhancement is weak. The rich spectroscopic features in TERS could also suggest PATP dimerization due to a strong local electromagnetic enhancement within the nanogap region of the tip-surface geometry. Moreover, the polarity of the bias voltage does not influence the TERS profiles in Figs. 2(a) and 2(b), which may indicate that the detected molecule should be structurally symmetric, offering additional evidence for the formation of DMAB converted from PATP to bridge two metal surfaces symmetrically (the Au tip and the Au film) with two thiol groups. Nevertheless, the difference between TERS and SERS spectra remains.

To interpret the above spectral phenomena correctly, we choose two spectra at different biases for vibrational mode assignments, as shown in Figs. 3(a) and 3(b). Furthermore, the Raman spectra of DMAB were calculated within density functional theory [26] using the GAUSSIAN 09 suite [27] with the PW91PW91 functional (Perdew-Wang's 1991 exchange functional plus Perdew-Wang's 1991s correlation functional) [28], a 6-31G(d) basis set for C, N, S, and H, and a LANL2DZ (Los Alamos National Laboratory 2 double  $\zeta$ ) basis set [29] for Au, where a  $\text{Au}_5$ -DMAB- $\text{Au}_5$  junction was used to simulate the Raman spectra, mimicking the TERS setup. The IR spectra of DMAB in the  $\text{Au}_5$ -DMAB- $\text{Au}_5$  junction were also simulated with the same method. Based on the simulated Raman spectrum in Fig. 3(c), all the Raman-active symmetric

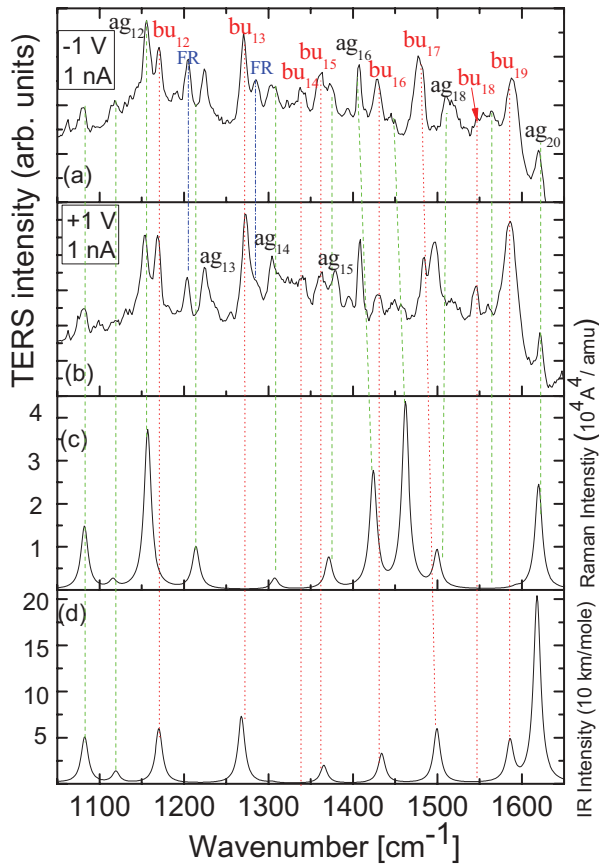


FIG. 3. (Color online) TERS peaks of DMAB under experimental conditions of 1 nA current and (a)  $-1$  V and (b)  $+1$  V bias voltage. (c) Simulated Raman and (d) IR spectra of DMAB, where the wave number is scaled by 1.014.

ag vibrational modes in Figs. 3(a) and 3(b) can be assigned. Interestingly, most of the remaining Raman peaks in Figs. 3(a) and 3(b) can be assigned as IR-active asymmetric bu modes according to the simulated IR spectrum in Fig. 3(d). It has been previously shown that the gradient-field effect can activate IR-active modes in SERS due to molecular quadrupole transitions when the molecules are placed near metal surfaces [22,23]. Such gradient-field effects were also observed in near-field optical microscopy Raman (NSOM-Raman) [24]. Similarly, the observation of the full activation of IR-active modes can be caused by very high field gradients within the nanogap of a highly asymmetric geometry, consisting of a sharp metal tip and a flat metal surface in our HV-TERS system. Moreover, the enormous electromagnetic field enhancement in the nanogap region makes this phenomenon of activation of IR-active modes more readily observable.

Next, we compare the simulated Raman spectrum in Fig. 3(c) and the SERS peaks in Fig. 2(c). It is found that six strong peaks in the experimental and simulated results agree well with each other without scaling. We also note that in the simulated Raman spectrum of DMAB in Fig. 3(c), the wave numbers have been scaled by an insignificant factor of 1.014 (or blueshifted by  $\sim 1\%$ ) for closer comparison with the TERS data shown in Figs. 3(a) and 3(b). Such blueshifts could easily

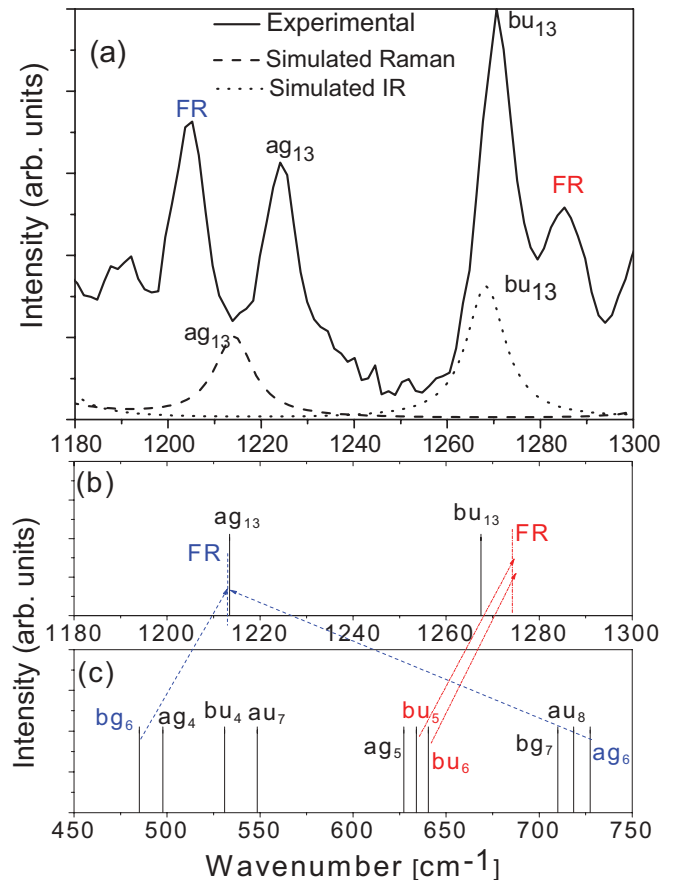


FIG. 4. (Color online) (a) Experimentally observed FR and simulated TERS peaks of DMAB for the Raman-active symmetric  $ag_{13}$  and IR-active asymmetric  $bu_{13}$  modes. (b) and (c) Calculated vibrational modes and the combinational modes for FR, where the wave number is scaled by 1.014.

be caused by weak external perturbations, such as tip, current, and voltage in the HV-TERS system.

Figure 4(a) shows a zoom-in spectrum of Fig. 3(a), where each of the symmetric and asymmetric C-N stretching modes, assigned as the Raman-active  $ag_{13}$  mode and IR-active asymmetric  $bu_{13}$  mode, respectively, splits into two Raman peaks. The splitting of the Raman peaks results from Fermi resonance (FR). In FR, an overtone of a different fundamental mode or a combination mode can appear in the vibrational spectra by gaining spectral weight from a fundamental mode [30]. FRs are frequently found in IR or Raman spectra in symmetric triatomic molecules such as  $CO_2$  and  $CS_2$  [30–32] but not in a TERS study. When the molecules are placed in the nanogap region, external perturbations from greatly enhanced electromagnetic fields, high field gradients, and the Au tip could cause such distinct FRs.

For a FR, the split vibrational energies under the perturbation can be written as [30–32]

$$E_{\pm} = \frac{1}{2}(E_A + E_B) \pm \frac{1}{2}\sqrt{(E_A - E_B)^2 + 4\phi^2}, \quad (1)$$

where  $E_A$  and  $E_B$  are the vibrational energies of the fundamental mode and an overtone of a different fundamental mode (or a combination mode) before splitting and  $\phi$  is the FR coupling coefficient, which describes the coupling strength

of the fundamental vibrational mode and the combinational mode (or the overtone mode) in the FR. When the FR coupling coefficient is larger, the spectral energy splitting between the fundamental vibrational mode and the combinational mode (or the overtone mode) is also larger. In addition, when the unperturbed energies  $E_A$  and  $E_B$  in Eq. (1) are closer, the FR coupling coefficient becomes larger. For our case in Fig. 4(a), the unperturbed energies  $E_A$  and  $E_B$  for the Raman-active symmetric  $ag_{13}$  or the IR-active asymmetric  $bu_{13}$  can be estimated as

$$E_A = \frac{E_+ + E_-}{2} + \frac{E_+ - E_-}{2} \frac{I_+ - I_-}{I_+ + I_-}, \quad (2)$$

$$E_B = \frac{E_+ + E_-}{2} - \frac{E_+ - E_-}{2} \frac{I_+ - I_-}{I_+ + I_-}, \quad (3)$$

where  $I_+$  and  $I_-$  are the Raman intensities of the split peaks. The difference in energy between the perturbed levels in the presence and absence of FR can be obtained with  $\Delta E_{\pm} = E_+ - E_-$  and  $\Delta E_{AB} = |E_A - E_B|$ , respectively.

In Fig. 4(a), we obtain  $I_+(ag_{13}) \approx I_-(ag_{13})$  and  $I_+(bu_{13}) \approx \frac{1}{2}I_-(bu_{13})$ ,  $\Delta E_{\pm}(ag_{13}) = 20.4 \text{ cm}^{-1}$ , and  $\Delta E_{\pm}(bu_{13}) = 14.6 \text{ cm}^{-1}$ . For the Raman-active symmetric  $ag_{13}$  mode, according to Eqs. (2) and (3), we obtain  $E_A = E_B = \frac{E_+ + E_-}{2}$ , i.e.,  $\Delta E_{AB} \approx 0 \text{ cm}^{-1}$ , and the FR coupling coefficient can be calculated by using Eq. (1) as  $\phi(ag_{13}) = \frac{1}{2}\Delta E_{\pm}(ag_{13}) = 10.2 \text{ cm}^{-1}$ . As illustrated in Figs. 4(b) and 4(c) with different vibrational modes marked as short vertical lines, the fundamental Raman-active symmetric  $ag_{13}$  mode frequency at  $1213 \text{ cm}^{-1}$  is very close to the combinational mode frequency of  $ag_6$  at  $727 \text{ cm}^{-1}$  and  $bg_6$  at  $485 \text{ cm}^{-1}$ . with  $\Delta E_{AB} = E(ag_{13}) - [E(bg_6) + E(ag_6)] \approx 1 \text{ cm}^{-1}$ . The combinational mode  $bg \times ag = bg$  is asymmetric.

For the IR-active asymmetric  $bu_{13}$  mode, we obtain  $E_A = \frac{E_+ + E_-}{2} + \frac{1}{3}\frac{\Delta E_{\pm}}{2}$  and  $E_B = \frac{E_+ + E_-}{2} - \frac{1}{3}\frac{\Delta E_{\pm}}{2}$ , according to Eqs. (2) and (3), and  $I_+(bu_{13}) \approx \frac{1}{2}I_-(bu_{13})$  as in Fig. 4(a). We can then obtain  $\Delta E_{AB}(bu_{13}) = \frac{1}{3}\Delta E_{\pm}(bu_{13}) = 4.9 \text{ cm}^{-1}$

and  $\phi(bu_{13}) = \frac{\sqrt{2}}{3}\Delta E_{\pm}(bu_{13}) = 6.88 \text{ cm}^{-1}$ . As illustrated in Figs. 4(b) and 4(c), the calculated IR-active asymmetric  $bu_{13}$  mode frequency at  $1267 \text{ cm}^{-1}$  is about  $7 \text{ cm}^{-1}$  smaller than the combinational mode of  $bu_5$  at  $634 \text{ cm}^{-1}$  and  $bu_6$  at  $640 \text{ cm}^{-1}$ . The difference between the experimental and theoretical values ( $4.9$  and  $7 \text{ cm}^{-1}$ ) is about  $2 \text{ cm}^{-1}$ . The symmetry of the combinational mode is  $bu \times bu = ag$  is symmetric.

In summary, by using the HV-TERS system, we have provided evidence for the conversion of PATP to DMAB via dimerization, possibly catalyzed by the presence of the TERS tip on top of the gold film. The observation in HV-TERS of the IR-active bands associated with DMAB molecules provides further experimental evidence for the dimerization mechanism. The activation of these extra modes is primarily attributed to enhanced electromagnetic field gradient effects within the gap region of the tip-surface geometry. Moreover, strongly enhanced plasmon responses in the nanogap region further result in distinct Fermi resonance to split the corresponding Raman peaks. These original findings not only are of fundamental significance but also help to significantly broaden the capacity of TERS as an analytical tool for ultrasensitive molecular spectroscopy.

#### ACKNOWLEDGMENTS

This work was supported by the National Basic Research Project of China (Grants No. 2012YQ12006005, No. 2009CB930701, No. 2009CB930704, and No. 2007CB936804), the National Natural Science Foundation of China (Grants No. 90923003, No. 10874233, No. 10874234, No. 20703064, No. 11034006, and No. 11227407), the Knowledge Innovation Project (Grant No. KJCX2-EW-W04) of CAS, the U.S. National Science Foundation (Grant No. 0906025), the U.S. Department of Energy, Basic Energy Sciences, Materials Sciences and Engineering Division, and the Nanometer Structure Consortium at Lund University, nmC@LU (H.X.X.).

- 
- [1] R. M. Stöckle, Y. D. Suh, V. Deckert, and R. Zenobi, *Chem. Phys. Lett.* **318**, 131 (2000).
- [2] N. Hayazawa, Y. Inouye, Z. Sekkat, and S. Kawata, *Opt. Commun.* **183**, 333 (2000).
- [3] M. S. Anderson, *Appl. Phys. Lett.* **76**, 3130 (2000).
- [4] B. Pettinger, B. Ren, G. Picardi, R. Schuster, and G. Ertl, *Phys. Rev. Lett.* **92**, 096101 (2004).
- [5] W. Zhang, X. Cui, B. S. Yeo, T. Schmid, C. Hafner, and R. Zenobi, *Nano Lett.* **7**, 1401 (2007).
- [6] E. Bailo and V. Deckert, *Chem. Soc. Rev.* **37**, 921 (2008).
- [7] J. Steidtner and B. Pettinger, *Phys. Rev. Lett.* **100**, 236101 (2008).
- [8] M. T. Sun, Z. L. Zhang, H. R. Zheng, and H. X. Xu, *Sci. Rep.* **2**, 647 (2012).
- [9] N. Jiang, E. T. Foley, J. M. Klingsporn, M. D. Sonntag, N. A. Valley, J. A. Dieringer, T. Seideman, G. C. Schatz, M. C. Hersam, and R. P. Van Duyne, *Nano Lett.* **12**, 5061 (2012).
- [10] M. Osawa, N. Matruda, K. Yoshii, and I. Uchida, *J. Phys. Chem.* **98**, 12702 (1994).
- [11] A. Campion and P. Kambhampati, *Chem. Soc. Rev.* **27**, 241(1998).
- [12] Q. Zhou, X. Li, Q. Fan, X. Zhang, and J. Zheng, *Angew. Chem., Int. Ed.* **45**, 3970 (2006).
- [13] T. Shegai, A. Vaskevich, I. Rubinstein, and G. Haran, *J. Am. Chem. Soc.* **131**, 14390 (2009).
- [14] D. Y. Wu, X. M. Liu, Y. F. Huang, B. Ren, X. Xu, and Z. Q. Tian, *J. Phys. Chem. C* **113**, 18212 (2009).
- [15] Y. R. Fang, Y. Z. Li, H. X. Xu, and M. T. Sun, *Langmuir* **26**, 7737 (2010).
- [16] Y. F. Huang, H. P. Zhu, G. K. Liu, D. Y. Wu, B. Ren, and Z. Q. Tian, *J. Am. Chem. Soc.* **132**, 9244 (2010).
- [17] M. T. Sun and H. X. Xu, *Small* **8**, 2777 (2012).
- [18] Y. Z. Huang, Y. R. Fang, Z. L. Yang, and M. T. Sun, *J. Phys. Chem. C* **114**, 18263 (2010).
- [19] W.-H. Park and Z. H. Kim, *Nano Lett.* **10**, 4040 (2010).
- [20] K. Kim, D. Shin, H. B. Lee, and K. S. Shin, *Chem. Commun.* **47**, 2020 (2011).

- [21] W. Ji, N. Spegazzini, Y. Kitahama, Y. Chen, B. Zhao, and Y. Ozaki, *J. Phys. Chem. Lett.* **3**, 3204 (2012).
- [22] M. Moskovits and D. P. DiLella, *J. Chem. Phys.* **73**, 6068 (1980).
- [23] M. Moskovits and D. P. DiLella, *J. Chem. Phys.* **77**, 1655 (1982).
- [24] E. J. Ayars, H. D. Hallen, and C. L. Jahncke, *Phys. Rev. Lett.* **85**, 4180 (2000).
- [25] B. Ren, G. Picardi, and B. Pettinger, *Rev. Sci. Instrum.* **75**, 837 (2004).
- [26] P. Hohenberg and W. Kohn, *Phys. Rev.* **136**, B864 (1964).
- [27] M. J. Frisch *et al.*, GAUSSIAN 09, revision A.02, Gaussian, Inc., Wallingford, CT, 2009.
- [28] J. P. Perdew, J. A. Chevary, S. H. Vosko, K. A. Jackson, M. R. Pederson, D. J. Singh, and C. Fiolhais, *Phys. Rev. B* **46**, 6671 (1992).
- [29] P. J. Hay and W. R. Wadt, *J. Chem. Phys.* **82**, 270 (1985).
- [30] E. Fermi, *Z. Phys.* **71**, 250 (1931).
- [31] R. A. Nyquist, H. A. Fouchea, G. A. Hoffman, and D. L. Hasha, *Appl. Spectrosc.* **45**, 860 (1991).
- [32] K. D. Bier and H. J. Jodi, *J. Chem. Phys.* **86** 4406 (1987).